journal

J. Am. Ceram. Soc., 98 [6] 1731–1738 (2015)
DOI: 10.1111/jace.13534

Impact of Stoichiometry on Structural and Optical Properties of Sputter Deposited Multicomponent Tellurite Glass Films

Okechukwu Ogbuu,[‡,†] Qingyang Du,[‡] Hongtao Lin,[‡] Lan Li,[‡] Yi Zou,[‡] Erick Koontz,[§] Charmayne Smith,[§] Sylvain Danto,[§] Kathleen Richardson,[§] and Juejun Hu[‡,†]

[‡]Department of Materials Science & Engineering, University of Delaware, Newark, Delaware 19716

[§]College of Optics and Photonics, CREOL, Department of Materials Science and Engineering, University of Central Florida, Orlando, Florida 32816

Multicomponent TeO_2–Bi_2O_3–ZnO (TBZ) glass thin films were prepared using RF magnetron sputtering under different oxygen flow rates. The influences of oxygen flow rate on the structural and optical properties of the resulting thin films were investigated. We observed that thin films sputtered in an oxygen-rich environment are optically transparent while those sputtered in an oxygen-deficient environment exhibit broadband absorption. The structural origin of the optical property variation was studied using X-ray diffraction, X-ray photoelectron spectroscopy, Raman Spectroscopy, and transmission electron microscopy which revealed that the presence of under-coordinated Te leads to the observed optical absorption in oxygen-deficient films.

I. Introduction

Tellurite glasses (containing TeO_2 as the main component) have attracted much attention for photonic applications due to their high refractive index ($n > 2$), large acousto-optic effect (three times that of quartz), singular nonlinear optical properties (e.g., their Raman coefficients are ~60 times higher than that of silica[1]), and can be tailored by knowledge of structural make-up,[2] excellent near- and mid-infrared transmittance (from around 400 nm to ~6 μm), large rare-earth solubility,[3–5] good chemical durability, and compatibility with fiber drawing processes.[6,7] Despite their hygroscopic nature which leads to loss when drawn into fibers,[8] they can be made into property-tailored transparent glass-ceramics[9] with specialized melting and heat-treatment protocols.[10] This set of unique properties make them strong candidates for applications in optical communications,[11] amplifiers, acousto-optic modulators,[12] light emitters,[3,4] lasers,[13] and optical storage devices.[14,15] Since TeO_2 under normal conditions does not have the ability to form glass structure easily, multicomponent tellurites, TeO_2-based glasses containing one or more chemical modifiers like alkali oxides, alkaline-earth oxides, or transition-metal oxides, are of great interest to the aforementioned applications given their much improved glass-forming ability [10,15,16] and enhanced optical properties.[17] The superior glass stability of multicomponent tellurites allows them to be prepared as bulk glass by melt quenching,[9,18,19] drawn into optical fibers,[15,20] and even remelted to form microspheres.[21] Planar tellurite thin films, on the other hand, constitute the basic building block for on-chip photonic devices such as waveguide amplifiers,[22] light emitters,[5] flexible photonic components,[23,24] and acousto-optical modulators. Multicomponent tellurite films have been prepared using sol–gel processing [25] and laser ablation.[26,27] Alternatively, radio-frequency (RF) magnetron reactive sputtering has been extensively used for oxide thin film deposition given its great versatility in controlling film stoichiometry, microstructure, and phase composition via tuning deposition parameters, in particular, oxygen partial pressure.[28–30] Thus far, the method has only been used to grow TeO_2 thin films,[11,28,31] Er-doped single-component TeO_2 films, and tungsten tellurite materials.[4,5]

Here, we explore RF reactive sputtering for multicomponent tellurite film preparation capitalizing on its unique ability to fine-tune resulting film stoichiometry and hence optical properties. Specifically, we choose TeO_2–Bi_2O_3–ZnO (TBZ) glass system as the addition of Bi_2O_3 and ZnO enhances glass polymerization by creating chain-like structures of Te–O–Te, and thereby increases the tendency of glass formation.[9,31] Consequently, this system exhibits superior glass stability and has been successfully used in low-loss optical fiber fabrication.[10,32] Unlike bulk glass processing or fiber drawing where composition variation during processing is usually minimal, vacuum deposition of thin films is highly susceptible to oxygen loss, and the resulting stoichiometry change has a major impact on film structure and properties. While the structure of bulk tellurite glasses has been investigated by several groups,[33–38] the structural properties of tellurite thin films, in particular the impact of glass stoichiometry, have been much less studied. In this study, we enumerate the experimental steps used to explore the film composition space by varying the deposition parameters, and discuss chemical, structural, and optical characterization results that elucidate the structure-optical property relation in the TBZ thin film system.

II. Experimental Details

(1) Sample Preparation

Glass target of composition $(TeO_2)_7$–Bi_2O_3–$(ZnO)_2$ [5.08 cm (2-in.) diameter; 0.635 cm (0.25 in.) thickness] were prepared by melt-quenching from commercial regents. Melt process optimization was carried out to ensure that robust, large diameter targets could be fabricated to enable deposition of desirable films with target thicknesses. Thin films were deposited from the target onto substrates (soda-lime silicate glass slides from Fisher Scientific Inc., Newark, DE or (100) silicon wafers from University Wafer Inc., Boston, MA) by RF reactive sputtering. The substrate choice has little impact on resulting film properties given the amorphous nature of the films. Hence, no changes were observed from characterization results performed on thin films deposited on both substrates. Before deposition, the glass substrates were cleaned with H_2SO_4-Nochromix® solution while silicon substrates

P. Lucas—contributing editor

Manuscript No. 35815. Received October 23, 2014; approved January 28, 2015.
[†]Author to whom correspondence should be addressed. e-mails: togbuu@udel.edu and hujuejun@udel.edu

were dipped into buffered oxide etch solution for 3 min to remove the native oxide layer. The sputter deposition chamber was first evacuated to a base pressure below 10^{-6} Torr. The target-substrate spacing is fixed at 13 cm for all deposition. Presputtering was conducted for 10 min prior to film deposition, with covered substrates, to clean the surface of the target of any possible contamination. Sputtering was performed, using a custom-designed system (PVD products), in oxygen (O_2) and argon (Ar) atmosphere with varying gas flow rates while keeping all other parameters constant to investigate the impact of oxygen stoichiometry change on film properties. The film deposition process parameters are summarized in Table I. The low sputtering power of 25 W is specific to tellurite targets to avoid target melting. The deposition rates shown in Table I were calibrated using a Dektak profilometer. The deposition rate decreases as the oxygen flow rate increases, which was similar to the report on Bi_2O_3.[30] The observed decrease in deposition rates with increasing oxygen content may be derived from the reduced level of energetic Ar+ ions in the plasma. During deposition, the substrates were rotated at 5 rpm to ensure uniform thin film deposition. For each deposition, the films are deposited on both soda-lime and Si substrates simultaneously. The substrates were not intentionally heated and were kept near room temperature throughout the deposition process. Depending on ratio of $Ar:O_2$ atmospheres, the sputtered films were labeled TBZ1 to TBZ4 as shown in Table I.

(2) Optical Measurements

Optical transmittance of the thin films deposited on soda-lime glass substrates were measured over a wavelength range 300–1800 nm using an ultraviolet–visible (UV-Vis) spectrophotometer (Perkin-Elmer 1050, Waltham, MA). Refractive index and extinction coefficient of the films were characterized using an M-44 rotating analyzer variable angle spectroscopic ellipsometer (VASE) (J.A. Woollam Co., Inc., Lincoln, NE) equipped with an autoretarder. Ellipsometry data were collected at three incidence angles: 62°, 67°, and 72° for TBZ1; 66°, 71°, and 76° for TBZ2; 69°, 74°, and 79° for TBZ3; and 66°, 71°, and 76° for TBZ4 which covers the (pseudo) Brewster angle for the tellurite thin films. Variable angle spectroscopic ellipsometry data were modeled using the Complete EASE®software (J.A Woollam Co., Lincoln, NE). B-spline function[39] was implemented to describe the dispersion of thin films sputtered in oxygen-rich atmosphere while Tauc-Lorentz model[40] was adapted to modeling the VASE data for thin film sputtered in oxygen-rich atmosphere.

(3) Morphological and Structural Characterization

The surface and cross-sectional morphology of the resulting tellurite films were examined using a JSM 7400F (JEOL co, Peabody, MA) scanning electron microscope (SEM) system operating with an accelerating voltage of 3 kV and transmission electron microscope (TEM) observations were taken on a JEM-2010F (JEOL co) system operating at an accelerating voltage of 200 KeV. The samples were covered with a thin (~30 nm) Au/Pd coating prior to SEM imaging to minimize charging from electron accumulation on the sample surface. Samples for TEM (thickness <100 nm) were prepared using focused ion beam on a Zeiss Auriga™ (San Diego, CA) crossbeam nanoprototyping station. Surface roughness of sputtered thin films was measured through atomic force microscopy (AFM) on a Dimension 3100 (Digital Instruments, Inc., Tonawanda, NY) microscope. Silicon AFM probes (Tap 150-G from Budget Sensors, Inc., Sofia, Bulgaria) with a force constant of 5 N/m and a resonant frequency of 150 KHz were used. The structural properties of the TBZ thin films deposited under different working gas (oxygen content) conditions were analyzed by glancing incident angle X-ray diffraction (GIXRD) using a Rigaku (Salem, NH) Ultima IV system equipped with CuK_α radiation (λ = 0.15406 nm) at 40 kV and 40 mA. Raman spectroscopy studies on TBZ thin films deposited on glass substrate were recorded using a DRX Raman microscope (AIY0900226) equipped with 10×, 50× objectives, a CCD detector and Rayleigh rejection filter. This system has a typical resolution of 2 cm^{-1} at room temperature and a backscattering geometry was used to collect the Raman signal. Before data collection, the system was calibrated with standard silicon wafers. An excitation wavelength of 532 nm was used, with an incident power of 2 mW. No damage was seen by 50× microscope inspection on film surfaces under these excitation conditions.

Table I. Deposition Parameters for Reactive Sputtering of Tellurite Films

Sample name	TBZ1	TBZ2	TBZ3	TBZ4
RF Power (W)	25	25	25	25
Sputtering pressure (mTorr)	2.5	2.5	2.5	2.5
$Ar:O_2$ flow rate (sccm)	17:0	15.3:1.7	13.6:3.4	11.9:5.1
Deposition rate (nm/min)	1.7	1.5	1.4	1.2

(4) Chemical Analysis

Compositional analysis was carried out using wavelength-dispersive spectroscopy (WDS) on a JXA-8200 electron microprobe analysis system (JEOL co). Three points were analyzed per sample in measuring the *k*-ratios of the samples. The X-ray lines and standards used for data analysis are as follows: Te: TeLα, Ag_2Te (Silver Telluride), Bi: BiMα, BGO (Bismuth Germanium Oxide), Zn: ZnKα, ZnO (Zinc Oxide), O: O Kα, BGO (Bismuth Germanium Oxide). The raw data were corrected for matrix effects with the PAP method using the General Motor Research film software thin-film analysis program. Chemical bonding states in TBZ thin films were examined using X-ray photoelectron spectroscopy (XPS). XPS spectra were recorded on an Omicron EA125 (Houston, TX) system equipped with dual aluminum–magnesium anodes using nonmonochromatic AlK_α ($h\nu$ = 1486.6 eV) radiation at room temperature and chamber vacuum below 2×10^{-7} Pa. Survey and high-resolution spectra were collected at constant analyzer energies 50 and 25 eV with step sizes of 1.0 and 0.05 eV, respectively.

III. Results and Discussions

TBZ thin films deposited in mixed Ar/O_2 atmosphere show drastically different appearance from those deposited in pure Ar plasma [Fig. 1(a)]. The former samples are optically transparent while the latter are opaque. Similar trends have been made on single-component TeO_2 films deposited by reactive sputtering.[11, 41] This observation indicates the important role film stoichiometry plays in dictating the film morphology and physical properties. Here, we evaluated the impact of oxygen deficiency on the structural, chemical, and optical properties of TBZ films to understand the structural origin of such drastic film appearance difference.

(1) Thin Film Optical Properties

Figure 1(b) shows the UV–Vis optical transmission spectra for bulk TBZ glass (in the form of a double side polished disk 6 mm in thickness) and TBZ thin films along with that of the glass substrate. All films sputtered in an Ar/O_2 environment (TBZ2-TBZ4) exhibit similar spectra, transparent to light above 350 nm wavelength (interference fringe maximums overlap with the glass substrate transmission spec-

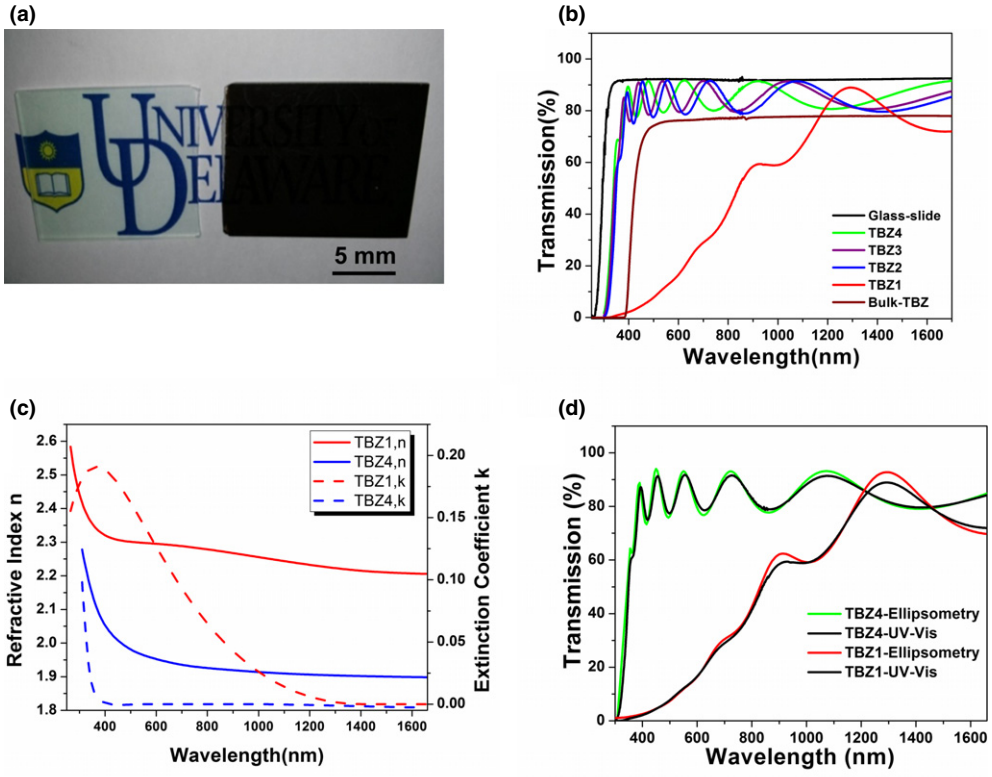

Fig. 1. (a) Photograph of TBZ4 (left) and TBZ1 (right) on University of Delaware logo for films on sodalime silicate glass substrates deposited under oxygen-rich (L) and deficient (R) conditions; (b) UV-Vis transmission spectrum of bulk TBZ & sputtered TBZ thin films superimposed on that of glass substrate with varying interference peaks showing thickness change; (c) Refractive index n and extinction coefficient k of sputtered thin films measured by ellipsometry; (d) Transmission spectrum comparing fitted ellipsometry model and UV-Vis data.

trum), whereas the film prepared in oxygen-deficient atmosphere (TBZ1) shows broadband optical absorption in the entire wavelength range measured, consistent with our visual inspection. This broad absorption in the entire visible spectrum indicates that oxygen deficiency defects may play a role in the opaqueness. This result is similar to the trend observed in RF magnetron sputtering of thin film TiO_2 [42,43] where increase in oxygen flow rate improves optical transmittance in TiO_2 films and shifts the optical absorption edge of the films to lower wavelengths. Varying interference fringe peaks in the spectrum indicates changes in growth rate as the oxygen flow rate increases. Figure 1(c) depicts the dispersion diagram measured using VASE. To validate the fitting model results from ellipsometry, the fitted *n* and *k* data were used as an input to a transfer matrix model to reproduce the optical transmission spectra measured by UV–Vis photo-spectrometry. Transmission spectra for the samples TBZ1 and TBZ4 simulated using the transfer matrix method were compared with their UV–Vis spectra as shown in Fig. 1(d). The excellent agreement confirms the validity of our ellipsometry fitting models.

(2) Thin Film Microstructure and Morphology

Figures 2(a) and (b) show SEM cross-sectional images of TBZ thin films deposited on silicon substrate at varying oxygen flow rates. The SEM cross-sectional images of all the thin films are similar in morphology but have different thickness. It can be seen that the thin films have a uniform and dense microstructure. Figures 2(c) and (d). show the TEM images of TBZ1 and TBZ4 films on silicon. The corresponding selected area electron-diffraction patterns show a diffuse broad diffraction ring approximately at same position indicating that both films are amorphous. The dark and bright spots present in TEM images are atomic columns confirming that a homogeneous amorphous phase is present in the thin films. The amorphous nature of all thin film samples was also confirmed using GIXRD: the spectra shown in Fig. 2(e) feature a broad peak centered at $2\theta = 28.1°$, consistent with previous reports on the bulk amorphous TeO_2–Bi_2O_3–ZnO system.[9] The results of thin film microstructure analysis, which asserts the amorphous nature of the sputtered TBZ films, are not surprising given the low substrate temperature. An average RMS value of (0.7 ± 0.02) nm was observed on the thin films.

(3) Compositional and Chemical Analysis

Compositions of the TBZ films as measured using WDS are tabulated in Table II with data uncertainties within ±0.6%. It was found that the elemental composition of Ar sputtered (TBZ1) thin films are close to the bulk target composition, where as films sputtered in Ar/O_2 environment become further oxidized. The latter finding is confirmed by the measured increase in oxygen concentration. It is interesting to note that (i) all the sputtered films have a Bi/Zn ratio of approximately 0.9 vs. 1 in the bulk glass and (ii) the Bi/Te and Zn/Te ratios in the Ar/O_2 sputtered films are also lower than the bulk glass but this is not the case for the TBZ1 film. Both observations are suggestive of a degree of preferential elemental sputtering. The conclusion was further confirmed by energy-dispersive X-ray (EDX) spectroscopy and XPS composition analysis.

XPS measurements were performed to elucidate the chemical state of elements in the bulk and thin films. Relatively low-resolution X-ray photoelectron survey scan in the binding energy region 0–1200 eV was recorded for each sample and a typical spectrum for the TBZ bulk and thin films is shown in Fig. 3(a). Peaks belonging to Tellurium, oxygen, bismuth, zinc and carbon were observed in the spectra. The presence of C1s peak at 284.6 eV, associated with postdeposition hydrocarbon contamination,[30, 44] is used as internal energy reference to determine the binding energy (B.E) of the XPS spectra. High-resolution spectra of Te3*d*, Bi4*f*, Zn2*p*, and O1*s* orbitals for TBZ bulk and thin films were collected.

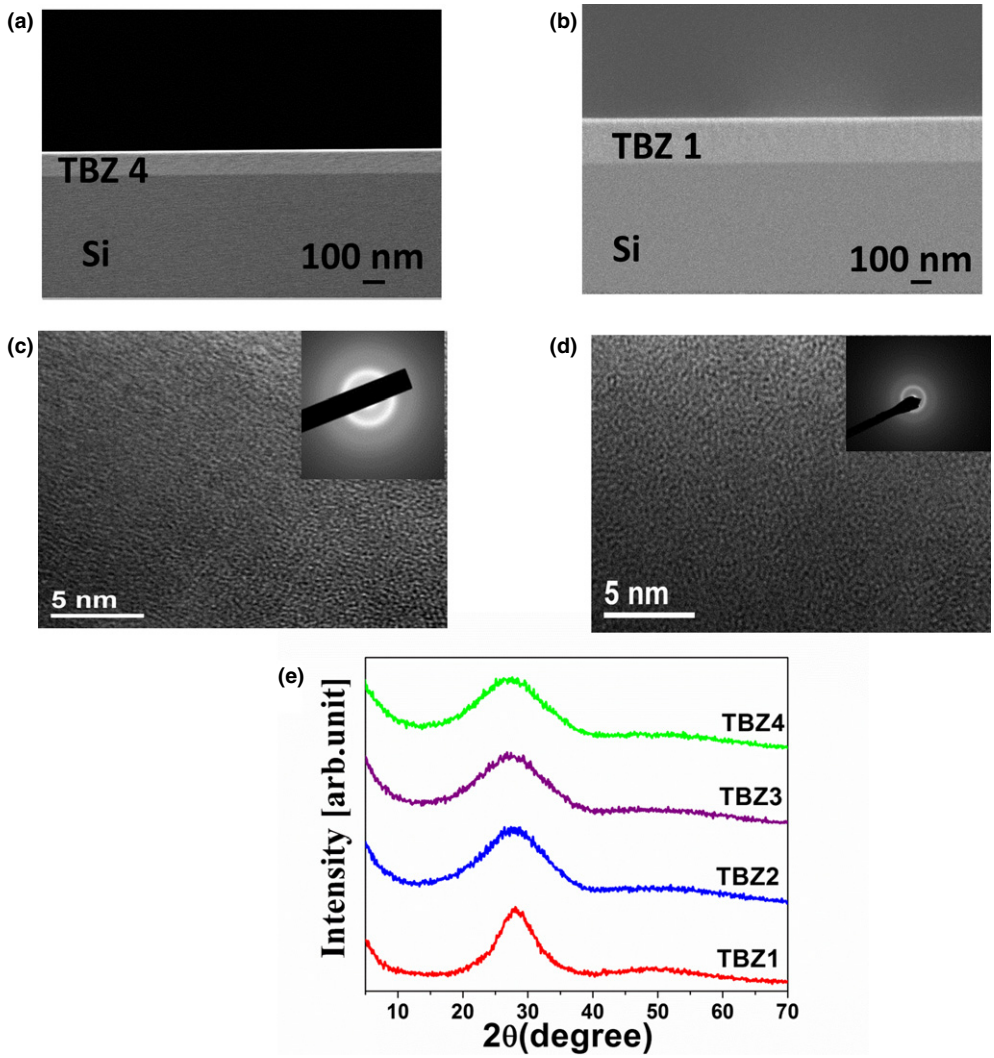

Fig. 2. SEM: Cross-sectional view of sputtered (a) TBZ4 & (b) TBZ1 on Silicon wafer; High resolution TEM images and selected area electron diffraction patterns (inset) of (c) oxygen-rich (TBZ4) (d) oxygen-poor (TBZ1) tellurite films;(e) Glancing incident angle X-ray diffraction spectra of TBZ thin film.

Table II. Atomic Composition of Sputtered Tellurite Films Measured Using Wavelength-Dispersive Spectroscopy

Sample ID	Te at.%	Bi at.%	Zn at.%	O at.%
Bulk	23.3	6.7	6.7	63.0
TBZ1	22.7	6.6	7.5	63.1
TBZ2	16.8	4.2	4.5	74.5
TBZ3	17.9	3.7	4.1	74.2
TBZ4	17.1	3.9	4.3	74.7

Peak fitting was performed using mixed Gaussian (70%)-Lorentzian (30%) curves, defined in the CasaXPS software® (CasaXPS Software, Dayton, OH) as GL(30), to obtain the peak positions and full width at half-maximum (FWHM). The curve fitting satisfies the following constraints: (a) orbitals relative peak area ratios; (b) each doublet has relatively equal FWHM; and (c) the spin orbit splitting of orbital.[45] The peak positions for core levels Te3*d*, Bi4*f*, Zn2*p* orbitals are listed in Table III while fitting details for Te3*d* orbitals are in Table IV.

Figures 3(b) and (c) show high-resolution spectra belonging to Zn2*p*, Bi4*f* orbitals in TBZ thin films at different deposition condition and TBZ bulk. Peaks centers associated with Bi4$f_{7/2}$, Bi4$f_{5/2}$, Zn2$p_{3/2}$, and Zn2$p_{1/2}$ for TBZ bulk and thin films were close to the reported values for Bi_2O_3[44,46] and ZnO.[47] The relative peak area ratio and spin-orbit coupling for Bi4$f_{7/2}$ and Bi4$f_{5/2}$ photolines were 3:4 and 5.3 eV, respectively while those for Zn2$p_{3/2}$ and Zn2$p_{1/2}$ photolines were 1:2 and 23.1 eV, respectively, in all samples investigated. Peaks of other oxides of bismuth and zinc were not observed and significant shift in core lines does not occur in the thin films grown in both oxygen-rich and -deficient atmosphere. This indicates that the oxidation state Bi^{3+} and Zn^{2+} were maintained in the oxides in all deposition conditions. Figure 3(d) shows high-resolution spectra corresponding O1s orbital for bulk-TBZ, TBZ1, and TBZ4. The slight asymmetry in O1s spectra in all samples is indicative of contributions from two different oxygen sites; bridging oxygen (BO) and nonbridging oxygen (NBO). The peaks associated with BO contributions were found at (531–532 eV) while those from NBO is found at (529–530 eV) similar to reported values for SiO_2- and TeO_2-based glasses.[48,49] The ratio of BO to NBO was found to increase as the oxygen flow rate in agreement with Raman spectra shown in the next section. Figures 3(e)–(g) shows the peaks corresponding to the doublets Te3$d_{3/2}$ and Te3$d_{5/2}$ for the bulk target, TBZ1 and TBZ4 thin films. The relative peak area ratio and spin-orbit coupling for Te3$d_{3/2}$ and Te3$d_{5/2}$ lines were 2:3 and 10.36 eV, respectively. Peak positions observed at (575.79–576.4) ± 0.02 eV and (586.16–586.75) ± 0.02 eV, respectively, correspond to those reported for amorphous TeO_2.[31,50] All patterns show a slight asymmetric line shape, suggesting the presence of mixed oxidation states of Te3*d* orbital.

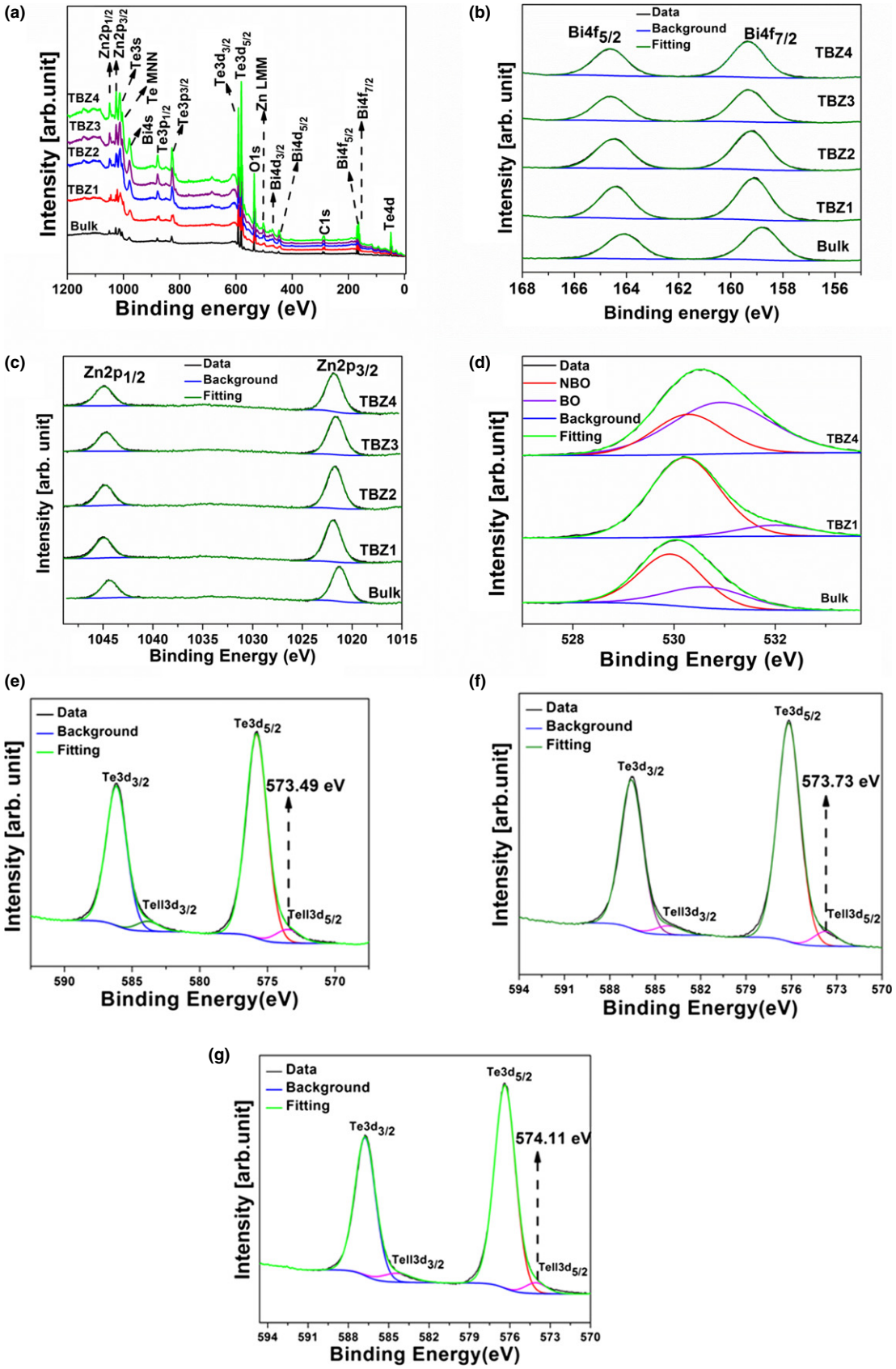

Fig. 3. XPS spectra showing (a) survey scan of all samples showing only the peaks belonging Te, O, Zn, and Bi orbitals; (b) deconvoluted high resolution scan of Bi4f orbital (c) deconvoluted high resolution scan of Zn2p orbital (d) deconvoluted high resolution scan of O1s orbital (e) deconvoluted high resolution scan of Te3d orbital for bulk (f) deconvoluted high resolution scan of Te3d orbital for TBZ1 (g) deconvoluted high resolution scan of Te3d orbital for TBZ4.

Previous reports on tellurite glasses assert that glass modifiers in TeO_2-based glass deform the TeO_4 structural units into TeO_3 with lower coordination number.[9,17] This deformation which easily occur along the axial-equatorial bonding of TeO_4 changes the Te_{ax}–O_{eq}–Te angle along the c-axis causing creation of defects, oxygen vacancies, and increases non-

Table III. Core Level Binding Energies of Tellurium, Bismuth, and Zinc in Bulk and Sputtered Tellurite Thin Films

	Binding energies (eV)				
	Bulk	TBZ1	TBZ2	TBZ3	TBZ4
Bi4$f_{7/2}$	158.80	159.12	159.23	159.32	159.33
Bi4$f_{5/2}$	164.11	164.42	164.51	164.62	164.63
Te3$d_{5/2}$	575.79	576.16	576.48	576.41	576.40
Te3$d_{3/2}$	586.16	586.56	586.84	586.77	586.75
Tell3$d_{5/2}$	573.49	573.73	574.07	574.10	574.11
Tell3$d_{3/2}$	583.84	584.13	584.39	584.55	584.41
Zn2$p_{3/2}$	1021.26	1021.93	1021.76	1021.64	1021.80
Zn2$p_{1/2}$	1044.36	1044.93	1044.79	1044.69	1044.90

Table IV. Details of the Curve Fitting of Te3*d* Core Level Spectra

		FWHM	Area	Background	Line shape
BULK	Te3*d*5/2	1.860	115082.4	Shirley	GL (30)
	Te3*d*3/2	1.814	76759.9	Shirley	GL (30)
	Tell3*d*5/2	2.141	8794.8	Shirley	GL (30)
	Tell3*d*3/2	1.957	5866.2	Shirley	GL (30)
TBZ1	Te3*d*5/2	1.791	106757.8	Shirley	GL (30)
	Te3*d*3/2	1.757	71207.5	Shirley	GL (30)
	Tell3*d*5/2	1.851	17061.4	Shirley	GL (30)
	Tell3*d*3/2	2.037	11380.0	Shirley	GL (30)
TBZ4	Te3*d*5/2	1.934	116497.8	Shirley	GL (30)
	Te3*d*3/2	1.897	77704.0	Shirley	GL (30)
	Tell3*d*5/2	1.11	4469.3	Shirley	GL (30)
	Tell3*d*3/2	1.11	2981.0	Shirley	GL (30)

bridging oxygen concentration, which is also confirmed by our Raman measurements to be discussed in the next section.[51] Oxygen vacancies result in creation of cation–cation bonds such as Te–Te and low coordinated Te.[52]

The Te–Te peaks at 573.73 eV[50,53] found in the oxygen-deficient film indicate the presence of under-coordinated Te which contributes to high absorption in the entire UV–Visible spectrum as observed in Fig. 1(b). The area of the shoulder peaks decreases and the binding energy increases as the oxygen in the environment increases. This suggests that the low coordinated Te present in oxygen-deficient thin films oxidizes and becomes TeO_2 and sub-oxides in the presence of oxygen, which explains the optical transparency of the oxygen-rich films.

(4) Impact of Stoichiometry on Thin Film Structure

To evaluate the structural evolution due to stoichiometry change, we resort to Raman spectroscopy to unravel the local cluster structures of tellurite glasses. Prior studies have shown that TeO_2-based glasses consist of asymmetric structural units such as TeO_4 trigonal bipyramid (tbp) and TeO_3 trigonal pyramid (tp).[33,35] Raman studies on single component TeO_2 assert that TeO_4 structural units with bridging oxygen dominate TeO_3 units in overall TeO_2 structure[54,5] However, it is observed that in multicomponent tellurite glasses TeO_3 units with nonbridging oxygen prevail over TeO_4 units because the addition of glass modifiers, such as Bi_2O_3 and ZnO, leads to the progressive transformation of TeO_4 structural units into TeO_3 units via the intermediate TeO_{3+1} units.[9]

To examine the influence of stoichiometric change in the structure of TBZ bulk and thin films, four Raman measurements recorded on different regions per sample were averaged and plotted in Fig. 4(a). The resulting spectra are deconvoluted using Gaussian fitting as shown in Fig. 4(b). The positions of the Raman bands of these glasses and their assigned vibrational modes are listed in Table V.

Three major features are observed from the measurements: TBZ-bulk target showed at 404, 652, 751 cm^{-1} while argon-sputtered thin film (TBZ1) displayed peaks, close to TBZ bulk target, around 392, 668, 750 cm^{-1}. Similarly, Raman peaks appeared in Ar/O_2-sputtered thin films around 463, 657, 769 cm^{-1}. The vibrational modes observed in our study can be associated with the following structural elements: (a) bands around 392–404 cm^{-1} are assigned to the bending mode of Te–O–Te linkages of predominant TeO_3 (tp) networks in TBZ-bulk target and TBZ1 while peaks located around 463 cm^{-1} belong to bending mode of Te–O–Te linkages of predominant TeO_4 (tbp) network in Ar/O_2-sputtered TBZ2-TBZ4 thin films[55,56]; (b) bands near 655–668 cm^{-1} belong to the vibration of the Te–O bonds in TeO_4 (tbp) with bridging oxygen (BO) or Te–O–Te linkages constructed by two unequal Te–O bonds[9,10,31]; (c) the band near 750–772 cm^{-1} originate from at least two main contributions assigned to stretching of Te–O or Te=O which contain nonbridging oxygen (NBO) in TeO_{3+1} or TeO_3 units.[9,10,55,57] The peak at 576 cm^{-1} originates from the soda-lime silicate glass substrate. As shown in Fig. 4(a), TeO_3 or TeO_{3+1} units with NBO are the predominant structural units in the bulk target and TBZ1 evident from their Raman peak intensity compared to those for TeO_4 units. The result is consistent with previous reports on bulk TBZ characterizations.[9,10] Apparently, as oxygen is introduced in the working gas, the stoichiometry of the thin films changes leading a different structural configuration with high concentration of BO. Consequently, the magnitude of peak intensity of band around 656–668 cm^{-1}, assigned to TeO_4 with bridging oxygen, increases as the oxygen flow rate leading to a shift in phonon mode of Te–O–Te linkages toward higher vibration frequency as seen in TBZ2-TBZ4. The structural evolution from bulk/TBZ1 to oxygen-rich thin films can be explained as for-

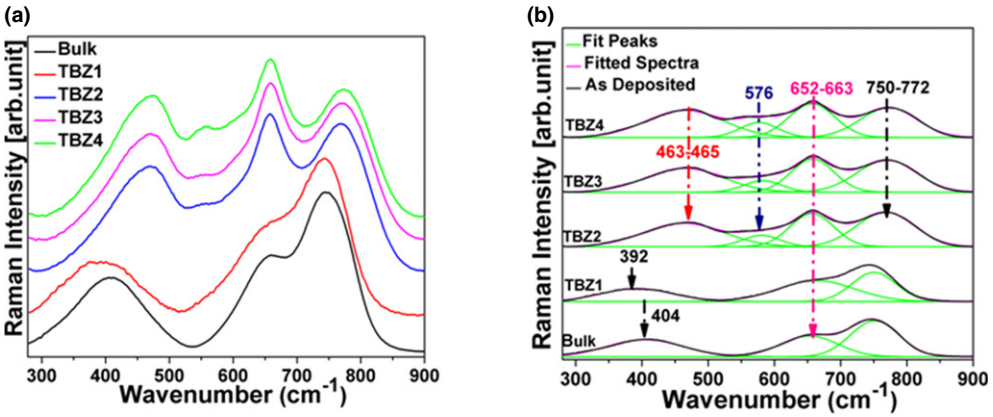

Fig. 4. (a) Raman spectra of tellurite thin films sputtered in varying argon and oxygen working gas; (b) Raman spectra decomposition into the respective vibrational modes. The corresponding peak assignments are listed in Table V.

Table V. Raman Peak Positions and Assignments

Raman band (cm^{-1})	Assignment
392–404	Bending mode of Te–O–Te linkage in TeO_3 network backbone in oxygen-deficient samples
463–465	Bending mode of Te–O–Te linkages in TeO_4 network backbone oxygen-rich samples
576	Contribution from the soda-lime substrate
656–657	Vibration of the Te–O bonds in TeO_4 trigonal bipyramid with bridging oxygen
750–772	Stretching mode of Te–O or Te=O which contain nonbridging oxygen (NBO) in TeO_{3+1} or TeO_3

mation of more TeO_4 structural units from TeO_3 units which indicate a change in coordination number of Te atoms from 3 to 4 ([TeO_3] tp) to ([TeO_4] tbp). Oxygen doping of TBZ-bulk target leads to the formation of Te–O bonds with large bond energy and force constant which is responsible for the Raman redshift.[41]

IV. Conclusion

In this report, we deposited planar TeO_2-based thin films using RF magnetron reactive sputtering. The effects of variation of oxygen flow rate in the working gas (Ar/O_2) on the structural, chemical state, and optical properties of sputtered thin film were thoroughly investigated using suitable characterization techniques. Thin films sputtered in Ar/O_2 atmosphere (oxygen-rich) possess large fractions of TeO_4 vibrational bonds and are structurally dissimilar to thin films deposited in pure argon atmosphere (oxygen-deficient) which contains large fractions of nonbridging oxygen. Increasing the oxygen flow rate improves the optical transparency in the multicomponent tellurite thin film in the entire visible and near-infrared region. We suggested that unoxidized Te element in oxygen-deficient thin films is responsible for the broad optical absorption. Understanding the structural and optical properties of sputtered planar tellurite thin films is expected to initiate the pathway for potential application in integrated photonics.

Acknowledgment

The authors thank funding support provided by the Department of Energy under award number DE-EE0005327.

References

[1]R. Jose and Y. Ohishi, "Enhanced Raman Gain Coefficients and Bandwidths in P_2O_5 and WO Added Tellurite Glasses for Raman Gain Media," *Appl. Phys. Lett*., **89** [12] 221122–5 (2006).

[2]G. Guery, A. Fargues, T. Cardinal, M. Dussauze, F. Adamietz, V. Rodriguez, and J. D. Musgraves, K. Richardson, and P. Thomas, "Impact of Tellurite-Based Glass Structure on Raman Gain," *Chem. Phys. Lett*., **554**, 123–7 (2012).

[3]A. Jha, S. Shaoxiong, H. Li Hui, and P. Joshi, "Spectroscopic Properties of Rare Earth Metal Ion Doped Tellurium Oxide Glasses and Fibres," *J. Opt*., **33**, 157–76 (2004).

[4]E. B. Intyushin and V. A. Novikov, "Tungsten-Tellurite Glasses and Thin Films Doped with Rare-Earth Elements Produced by Radio Frequency Magnetron Deposition," *Thin Solid Films*, **516** [12] 4194–200 (2008).

[5]P. T. Lin, M. Vanhoutte, N. S. Patel, V. Singh, J. Hu, Y. Cai, R. Camacho-Aguilera, J. Michel, L. C. Kimerling, and A. Agarwal, "Engineering Broadband and Anisotropic Photoluminescence Emission from Rare Earth Doped Tellurite Thin Film Photonic Crystals," *Opt. Express*, **20** [3] 2124–35 (2012).

[6]R. A. Myers, N. Mukherjee, and S. R. J. Brueck, "Large Second-Order Nonlinearity in Poled Fused Silica," *Opt. Lett*., **16**, 1732–4 (1991).

[7]S. H. Kim and T. Yoko, "Nonlinear Optical Properties of TeO_2-Based Glasses: MO_x-TeO_2 (M = Sc, Ti, V, Nb, Mo, Ta and W) Binary Glasses," *J. Am. Ceram. Soc*., **78** [4] 1061–5 (1995).

[8]G. Guery, T. Cardinal, A. Fargues, V. Rodriguez, M. Dussauze, D. Cavagnat, P. Thomas, J. Cornette, P. Wachtel, J. D. Musgraves, and K. Richardson, "Influence of Hydroxyl Group on IR Transparency of Tellurite- Based Glasses", *Int. J. Appl. Glass Sci*., 1–7 (2013).

[9]X. Hu, G. Guery, J. Boerstler, J. D. Musgraves, D. Vanderveer, P. Wachtel, and K. Richardson, "Influence of Bi_2O_3 Content on the Crystallization Behavior of TeO_2-Bi_2O_3-ZnO Glass System," *J. Non-Crystall. Solids*, **358**, 952–8 (2012).

[10]J. Massera, A. Haldeman, D. Milanese, H. Gebavi, M. Ferraris, P. Foy, W. Hawkins, J. Ballato, R. Stolen, L. Petit, and K. Richardson, "Processing and Characterization of a Core-Clad Tellurite Glass Preforms and Fibers Fabricated by Rotational Casting," *J. Opt. Mater*., **32** [5] 582–8 (2010).

[11]S. Madden and K. T. Vu, "Very Low Loss Reactively Ion Etched Tellurium Dioxide Planar Rib Waveguides for Linear and Non-Linear Optics," *Opt. Express*, **17**, 20–17645 (2009).

[12]R. A. H. El-Mallawany, *Tellurite Glasses Handbook*, p. 113. CRC Press, Boca Raton, FL, 2000.

[13]B. Richards, A. Jha, Y. Tsang, D. Binks, J. Lousteau, F. Fusari, A. Lagatsky, C. Brown, and W. Sibbett, "Tellurite Glass Lasers Operating Close to 2 μm," *Laser Phys. Lett*., **7** [3] 177–93 (2010).

[14]K. Tanaka, A. Narazaki, K. Hirao, and N. Soga, "Optical Second Harmonic Generation Inpoled MgO–ZnO–TeO_2 and B_2O_3–TeO_2 Glasses," *J. Non-Cryst. Solids*, **203**, 49–54 (1996).

[15]J. S. Wang, E. M. Vogel, and E. Snitzer, "Tellurite Glass: A New Candidate for Fiber Devices," *Opt. Mater*., **3** [3] 187–203 (1994).

[16]M. R. Oermann, H. Ebendorff-Heidepriem, Y. Li, T. Foo, and T. M. Monro, "Index Matching Between Passive and Active Tellurite Glasses for Use in Microstructure Fiber Lasers: Erbium Doped Lanthanum-Tellurite Glass," *Opt. Express*, **17** [18] 15578–84 (2009).

[17]C. Rivero, R. Stegeman, K. Richardson, G. Stegeman, G. Turri, M. Bass, P. Thomas, M. Udovic, T. Cardinal, E. Fargin, M. Couzi, H. Jain, and A. Miller, "Influence of Modifier Oxides on the Structural and Optical Properties of Binary TeO_2 Glasses," *J. Appl. Phys*., **101** [2] 023526–7 (2007).

[18]E. Yousef, M. Hotzel, and C. Rüssel, "Effect of ZnO and Bi_2O_3 Addition on Linear and Non-Linear Optical Properties of Tellurite Glasses," *J. Non-Cryst.Solids*, **353**, 333–8 (2007).

[19]R. Jose and Y. Ohishi, "Higher Non-Linear Indices, Raman Gain Coefficients and Bandwidths in the TeO_2-ZnO-NbO_5-MoO_3 Quaternary Glass System," *Appl. Phys. Lett*., **90**, 211104–3 (2007).

[20]M. R. Henderson, B. C. Gibson, H. Ebendorff-Heidepriem, K. Kuan, S. V. Afshar, J. O. Orwa, I. Aharonovich, S. Tomljenovic-Hanic, A. D. Greentree, S. Prawer, and T. M. Monro, "Diamond in Tellurite Glass: A New Medium for Quantum Information," *Adv. Mater*., **23**, 2806–10 (2011).

[21]Y. Ruan, K. Boyd, H. Ji, A. Francois, H. Ebendorff- Heidepriem, J. Munch, and T. M. Monro, "Tellurite Microspheres for Nanoparticle Sensing and Novel Light Sources," *Opt. Express*, **22** [10] 11995–2006 (2014).

[22]J. I. Mackenzie, G. S. Murugan, A. W. Yu, and J. B. Abshire, "Er-Doped Tellurite Waveguides for Power Amplifiers," *Proc. SPIE 8988, Integr. Optics: Devices Mater. Technol*., **XVIII**, 898809-7 (2014).

[23]L. Li, H. Lin, S. Qiao, Y. Zou, S. Danto, K. Richardson, J. David Musgraves, N. Lu, and J. Hu, "Integrated Flexible Chalcogenide Glass Photonic Devices," *Nat. Photonics*, **8**, 643–9 (2014).

[24]J. Hu, L. Li, H. Lin, P. Zhang, W. Zhou, and Z. Ma, "Flexible Integrated Photonics: Where Materials, Mechanics and Optics Meet [Invited]," *Opt. Mater. Express*, **3**, 1313–31 (2013).

[25]L. Weng, S. N. B. Hodgson, and J. Ma, "Preparation of TeO_2-TiO_2 Thin Films by Sol-Gel Process," *J. Mater. Sci. Lett*., **18**, 2037–9 (1999).

[26]M. Bouazaoui, B. Capoen, A. P. Caricato, A. Chiasera, A. Fazzi, M. Ferrari, G. Leggieri, M. Martino, M. Mattarelli, M. Montagna, F. Romano, T. Tunno, S. Turrel, and K. Vishnubhatla, "Pulsed Laser Deposition of Er-Doped Tellurite Films on Large Area," *J. Phys: Conf. Ser*., **59**, 475–8 (2007).

[27]A. P. Caricato, M. Fernández, M. Ferrari, G. Leggieri, M. Martino, M. Mattarelli, M. Montagna, V. Resta, L. Zampedri, R. M. lmeida, M. C. Conçalves, L. Fortes, and L. F. Santos, "Er^{3+}-Doped Tellurite Waveguides Deposited by Excimer Laser Ablation," *Mat. Sci. Eng. B*, **105**, 65–69 (2003).

[28]F. D'Amore, M. Di Giulio, S. M. Pietralunga, A. Zappettini, L. Nasi, V. Rigato, and M. Martinelli, "Sputtered Stoichiometric TeO_2 Glass Films: Dispersion of Linear and Nonlinear Optical Properties," *J. Appl. Phys*., **94**, 1654–61 (2003).

[29]M. D. Giulio, M. C. Nicotra, M. Re, R. Rella, and P. Siciliano, "Optical Absorption and Structural Characterization of Reactively Sputtered Tellurium Suboxide Thin Films," *Appl. Surf. Sci*., **65/66**, 313–8 (1993).

[30]H. T. Fan, S. S. Pan, X. M. Teng, C. Ye, G. H. Li, and L. D. Zhang, "Δ-Bi_2O_3 Thin Films Prepared by Reactive Sputtering: Fabrication and Characterization," *Thin Solid Films*, **513**, 142–7 (2006).

[31]N. Dewan, V. Guputa, K. Sreenivas, and R. S. Katiyar, "Growth of Amorphous TeO_x($2 < x < 3$) Thin Film by Radio Frequency Sputtering," *J. Appl. Phys*., **101**, 084910–7 (2007).

[32]J. Massera, A. Halderman, J. Jackson, C. Rivero-Baleine, L. Petit, and K. Richardson, "Processing of Tellurite-Based Glass with Low OH Content," *J. Am. Ceram. Soc*., **94** [1] 130–6 (2011).

[33]M. Tatsumisago, S. K. Lee, T. Minami, and Y. Kowada, "Raman Spectra of TeO_2-Based Glasses and Glassy Liquids: Local Structure Change with Temperature in Relation to Fragility of Liquid," *J. Non-Cryst. Solids*, **177**, 154–63 (1994).

[34]J. Heo, G. H. Sigel Jr., E. A. Mendoza, and D. A. Hensley, "Spectroscopic Analysis of the Structure and Properties of Alkali Tellurite Glasses," *J. Am. Ceram. Soc*., **75**, 277–81 (1992).

[35]T. Sekiya, N. Mochida, A. Ohtsuka, and M. Tonokawa, "Raman Spectra of $MO_{1/2}$-TeO_2 (M=Li, Na, K, Rb, Cs,and Tl) Glasses," *J. Non-Cryst. Solids*, **144**, 128–44 (1992).

[36]J. Jackson, C. Smith, J. Massera, C. Rivero-Baleine, C. Bungay, L. Petit, and K. Richardson, "Estimation of Peak Raman Gain Coefficients for

Barium-Bismuth-Tellurite Glasses from Spontaneous Raman Cross-Section Experiments," *Opt. Express*, **17**, 9071–9 (2009).

[37]M. A. Salim, G. D. Khattak, N. Tabet, and L. E. Wenger, "X -Ray Photoelectron Spectroscopy (XPS) Studies of Copper–Sodium Tellurite Glasses," *J. Electron Spectrosc. Relat. Phenom.*, **128**, 75–83 (2003).

[38]A. Osaka, Q. Jianrong, T. Nanba, Y. Miura, and T. Yao, "EXAFS of Tellurium in the Glasses of B_2O_3-TeO_2 System," *J. Non-Cryst. Solids*, **142**, 81–6 (1992).

[39]J. W. Weber, T. A. R. Hansen, M. C. M. van de Sanden, and R. Engeln, "B-Spline Parameterization of the Dielectric Function Applied Spectroscopic Ellipsometry on Amorphous Carbon," *J. Appl. Phys.*, **106**, 123503–9 (2009).

[40]G. E. Jellison and F. A. Modine, "Parameterization of the Optical Functions of Amorphous Materials in the Interband Region," *Appl. Phys. Lett.*, **69**, 371–3 (1996).

[41]R. Nayak, V. Gupta, A. L. Dawar, and K. Sreenivas, "Optical Waveguiding in Amorphous Tellurium Oxide Thin Films," *Thin Solid Films*, **445**, 118–26 (2003).

[42]C. H. Heo, S. Lee, and J. Boo, "Deposition of TiO_2 Thin Films Using RF Magnetron Sputtering Method and Study of Their Surface Characteristics," *Thin Solid Films*, **475**, 183–8 (2005).

[43]M. Chandra Sekhar, P. Kondaiah, B. Radha Krishna, and S. Uthanna, "Effect of Oxygen Partial Pressure on the Electrical and Optical Properties of DC Magnetron Sputtered Amorphous TiO_2 Films," *J. Spectrosc.*, **213**, 462734–7 (2013).

[44]G. E. Mullenberg (ed), *Handbook of X-ray Photoelectron Spectroscopy*. Perkin-Elmer, Norwalk, CT, 1970.

[45]T. S. Sian and G. B. Reddy, "Optical, Structural and Photoelectron Spectroscopic Studies on Amorphous and Crystalline Molybdenum Oxide Thin Films," *Sol. Energy Mater. Sol. Cells*, **82**, 375–86 (2004).

[46]W. E. Morgan, W. J. Stec, and J. R. Van Wazer, "Inner-Orbital Binding-Energy Shifts of Antimony and Bismuth Compounds," *Inorg. Chem.*, **12** [4] 953–5 (1973).

[47]C. D. Wagner, W. M. Riggs, L. E. Davis, J. F. Moulder, and G. E. Muilenberg, *Handbook of X-ray Photoelectron Spectroscopy*. Perkin-Elmer Corporation, Physical Electron Division, Eden Prairie, MN (1979).

[48]H. W. Nesbitt, G. M. Bancroft, G. S. Henderson, R. Ho, K. N. Dalby, Y. Huang, and Z. Yan, "Bridging, non-Bridging and Free (O^{-2}) Oxygen in Na_2O-SiO_2 Glasses: An X-ray Photoelectron Spectroscopic(XPS) and Nuclear Magnetic Resonance (NMR) Study," *J. Non-Cryst. Solids*, **357**, 170–80 (2011).

[49]G. D. Khattak, A. Mekki, and L. E. Wenger, "Local Structure and Redox State of Copper in Tellurite Glasses," *J. Non-Cryst. Solids*, **377**, 174–81 (2004).

[50]A. J. Ricco, H. S. White, and M. S. Wrighton, "X-ray Photoelectron and Auger Electron Spectroscopic Study of the CdTe Surface Resulting from Various Surface Pretreatments: Correlation of Photo-Electrochemical and Capacitance-Potential Behavior with Surface Chemical Composition," *J. Vac. Sci. Techol. A*, **2**, 910–6 (1984).

[51]R. El-Mallawany, A. Abdel-Kader, M. El-Hawary, and N. El-Khoshkhany, "UV-IR Spectra of New Tellurite Glasses," *Eur. Phys. J. AP*, **19**, 165–72 (2002).

[52]V. K. Tikhomirov, A. B. Seddon, D. Furniss, and M. Ferrari, "Intrinsic Defects and Glass Stability in Er^{3+}-Doped TeO_2 Glasses and the Implications for Er^{3+}-Doped Tellurite Fiber Amplifiers," *J. Non-Cryst. Solids*, **326**, 296–300 (2003).

[53]M. DiGiulio, G. Micocci, R. Rella, P. Sicilano, and A. Tewre, "Optical Absorption of Tellurium Suboxide Thin Films," *Phys. Stat. Sol (a)*, **136**, K101 (1993).

[54]B. Jeansannetas, S. Blanchandin, P. Thomas, P. Marchet, J. C. Champarnaud-Mesjard, T. Merle-MeHjean, B. Frit, V. Nazabal, E. Fargin, G. Le Flem, M. O. Martin, B. Bousquet, L. Canioni, S. Le Boiteux, P. Segonds, and L. Sarger, "Glass Structure and Optical Nonlinearities in Thallium(I) Tellurium(IV) Oxide Glasses," *J. Solid State Chem.*, **146**, 329–35 (1999).

[55]A. P. Mirgorodsky, T. Merle-Mejean, J. C. Champarnaud, P. Thomas, and B. Frit, "Dynamics and Structure of TeO_2 Polymorphs: Model Treatment of Paratellurite and Tellurite; Raman Scattering Evidence for new γ- and δ – Phases," *J. Phys. Chem. Solids*, **61**, 501–9 (2000).

[56]S. O. Baki, L. S. Tan, C. S. Kan, H. M. Kamari, A. S. M. Noor, and M. A. Mahdi, "Structural and Optical Properties of Er^{3+}-Yb^{3+} Codoped Multicomposition TeO_2-ZnO-PbO-TiO_2-Na_2O Glass," *J. Non-Cryst. Solids*, **362**, 156–61 (2013).

[57]J. Ozdanova, H. Ticha, and L. Tichy, "Remark on the Optical Gap in ZnO-Bi_2O_3-TeO_2 Glasses," *J. Non-Cryst. Solids*, **353**, 2799–802 (2007). □